CHAPTER 2

ELASTICITY OF OXIDES AND IONICS

Lars Stixrude
Department of Geological Sciences, University of Michigan, Ann Arbor, Michigan, USA

Contents

ABSTRACT

The elastic constants are important for understanding the response of materials subject to small- or high- frequency strains, and for understanding the relationship between crystal structure and bonding. Subtleties arise in the definition of the elastic constants particularly in the case of nonvanishing prestress. We review some of the definitions of the elastic constants that have appeared in the literature and discuss the important distinctions among them including the stress-strain, energy-strain, and wave propagation coefficients. The Born stability criteria, the Cauchy conditions, and elastic wave propagation are discussed in this context. The limits of elastic behavior are explored in the context of attenuation and low-frequency behavior and in the comparison of the elasticity of fluids and solids. New developments in the theory and computation of the elastic constants are discussed, focusing on the contributions of density functional theory, and contrasting this first-principles approach with more approximate ab initio and semi-empirical treatments that have played an important role in the study of elasticity. The behavior of the elastic constants of a wide range of materials is illustrated. The transition metals show the effects of the electronic structure on the elastic constants, including the effects of d-band filling, strain splitting, and the role of magnetism. The oxides show that sublattice displacements may have a large influence on the elastic constants and may be responsible for elastic instabilities and phase transitions, as in the case of the stishovite to $CaCl_2$ structure transition in silica. Elastic anisotropy is illustrated with results from density functional theory, and also with a

Handbook of Elastic Properties of Solids, Liquids, and Gases, edited by Levy, Bass, and Stern
Volume II: Elastic Properties of Solids: Theory, Elements and Compounds, Novel Materials, Technological Materials, Alloys, and Building Materials

ISBN 0-12-445762-2 / $35.00

simple central nearest-neighbor force model that accounts for many important features of the elasticity of elements. The effect of pressure on the elastic constants is examined as are the consequences for the elastic anisotropy which is seen to depend qualitatively (in sense as well as magnitude) on pressure.

2.1. INTRODUCTION

The subject of elasticity is important in many fields, including those in which an understanding of the deformation of materials at high frequency or small magnitude is important. In the earth sciences, elasticity lies at the heart of our understanding of the earthquake process and of the structure of the earth's interior. The otherwise inaccessible depths are revealed to us through the generation and propagation of elastic (seismic) waves. The earth is an extraordinary laboratory for the study of elasticity on length scales ranging from single crystals to our planet itself, and time scales ranging from earthquakes to the viscoelastic regime probed by mantle convection and the earth's self-gravitation.

Elasticity provides fruitful ground for an exploration of the foundations of material behavior in the relationship between crystal structure and bonding. The fourth-ranked elastic constant tensor is unusually rich in this regard and reflects the symmetry of the underlying structure. For example, the contrast between periodic and nonperiodic condensed matter is immediately apparent in the elastic anisotropy, a distinction that is not as clear cut in tensorial properties of lower rank such as the dielectric constant, which is isotropic for cubic and nonperiodic materials alike.

The foundations of the microscopic theory of elasticity were laid some time ago in work by Born and Huang [1], followed by other excellent treatments [2]. Many details, however, remain troublesome and continue to cause confusion in the literature. When dealing with elasticity, details matter in ways that can be surprising. For example, expanding the free energy in the displacement gradient instead of the strain produces elastic moduli with different symmetry properties; the elastic constants in a material subject to prestress have case here, that of hydrostatic prestress. This is the relevant case in many situations including most laboratory studies and the interior of the earth below the upper thermal boundary layer (lithosphere). The strain will also be separated into a large finite deformation associated with the prestress, and an infinitesimal strain associated with the incremental stress. Our discussion follows that of [11].

Consider a material point that can be located with respect to Cartesian axes. In the natural or unstressed state, its location is described by the vector a. Its position after the application of prestress is denoted by X and after the application of the further infinitesimal stress by x. The relationship between the prestressed and final positions is given by the displacement

$$u_i = x_i - X_i \tag{2.1}$$

We assume that there exists a unique, linear, one-to-one mapping between natural, prestressed, and final coordinates that may be described by the displacement gradients, u, v, and w,

$$x_i - X_i = u_{ij} X_j \tag{2.2}$$

$$x_i - a_i = v_{ij} a_j = w_{ij} x_j \tag{2.3}$$

where the definition of v implies a Lagrangian frame of reference, and the definition of w an Eulerian frame.

The displacement gradients contain contributions from deformation and from rotation. For the infinitesimal displacement gradients u, these are identified with,

respectively, the symmetric and antisymmetric parts

$$\epsilon_{ij} = \tfrac{1}{2}(u_{ij} + u_{ji}) \tag{2.4}$$

$$\omega_{ij} = \tfrac{1}{2}(u_{ij} - u_{ji}) \tag{2.5}$$

suffered multiple definitions [3]. It is because of this confusion that some care has been taken here to define stress and strain tensors and the elastic constants that relate them. Much of this discussion follows the outstanding work of Wallace [4].

Among important recent developments has been the ability to compute the elastic constants from first-principles band-structure calculations. The development and documentation of the success of density functional theory [5, 6], the development of the plane-wave pseudopotential method [7], the ability to efficiently compute forces and stresses [8] as well as the total energy, and to rapidly determine equilibrium structures [9, 10] have all contributed to this development. Included here is a brief description of these methods and a comparison with other microscopic methods of computing elasticity, including the rigid ion-pair potentials that played such an important role in early work, and the ab initio models that occupy an intermediate position in the continuum from semi-empirical to first-principles approaches.

After a review of theory, we consider a few examples of the elastic behavior of materials. Included are those that show the relationship between the electronic structure and the elastic constants (the transition metals), the influence of crystal structure (oxides), and the effect of high pressure. Also shown are examples of behavior that are likely to be found in many materials including the strong dependence of the elastic anisotropy on pressure, and the importance of sublattice displacements (sometimes still overlooked) on the elastic constants.

2.2. ELASTICITY

2.2.1. Strain and Stress Tensors

The elastic constants relate applied external forces, described by the stress tensor, to the resulting deformation, described by the strain tensor. We view a crystal as a homogeneous anisotropic medium and assume that stress and strain are homogeneous. One divides the stress into two parts, a prestress and a further infinitesimal stress. We will focus on a special where ϵ_{ij} is the infinitesimal or Cauchy strain tensor and ω_{ij} is the rotation tensor. The strain tensor is defined to be positive for expansion.

The strain associated with prestress will be finite in general. In contrast to the infinitesimal case, a unique definition of the finite strain tensor is not possible. The reason is that the displacement gradients v and w are not frame-indifferent. Consider the change in length of a line element

$$|dx|^2 - |da|^2 = 2e_{ij}\,dx_i\,dx_j = 2\eta_{ij}\,da_i\,da_j \tag{2.6}$$

where the Einstein summation convention has been assumed. These relations define the Eulerian (e) and Lagrangian (η) finite strain tensors. Evaluation of the change in length leads to the following expressions

$$e_{ij} = \tfrac{1}{2}(w_{ij} + w_{ji} - w_{ij}w_{jk}) \tag{2.7}$$

$$\eta_{ij} = \tfrac{1}{2}(v_{ij} + v_{ji} + v_{ij}v_{jk}) \tag{2.8}$$

In the limit of small strains, the nonlinear terms vanish and these two measures of strain are equivalent, both reducing to the Cauchy strain tensor (Eq. 1.4). However, for finite strains, they differ so that constitutive relations will not be frame-indifferent. This has

important implications for the representation and description of physical properties at high pressure including the equation of state [12].

The stress tensor at a point in a body can be defined through the expression relating the components of the traction, t acting on the surface elements dS

$$t_i = \sigma_{ij}\, dS_j \tag{2.9}$$

Some care must be taken in the definition [4]. We take the tractions to be those acting on the initial state and the surface elements those of the initial, undeformed configuration. In this case, the stress tensor σ_{ij} is the second Pirola–Kirchoff stress [13]. This stress tensor is symmetric, corresponding to vanishing torques acting on the crystal. The components with $i = j$ are the normal components of stress (positive for tensile stresses) and the components with $i \neq j$ are the shear components.

2.2.2. Elastic Constants

The stress tensor can also be defined in terms of the change upon deformation of an appropriate thermodynamic potential. This definition, which will also lead to the expression for the elastic constants, places the elasticity within the same framework of other thermodynamic properties of the crystal, such as the equation of state and the entropy. These may all be expressed in terms of the derivatives of the potential with respect to its natural variables [4]. For example, the stress produced by a deformation under isothermal conditions is

$$\sigma_{ij} = \rho \left(\frac{\partial A}{\partial \epsilon_{ij}} \right)_T \tag{2.10}$$

while that produced under isentropic conditions is

$$\sigma_{ij} = \rho \left(\frac{\partial E}{\partial \epsilon_{ij}} \right)_S \tag{2.11}$$

where A is the Helmholtz free energy, E is the internal energy, ρ is the density, and the subscripts on the derivatives indicate that temperature or entropy is to be held constant.

The elastic constants are defined in terms of the Hooke's law relation between stress and strain. The isothermal and adiabatic elastic constants are given by, respectively,

$$c^T_{ijkl} = \left(\frac{\partial \sigma_{ij}}{\partial \epsilon_{kl}} \right)_T \tag{2.12}$$

$$c^S_{ijkl} = \left(\frac{\partial \sigma_{ij}}{\partial \epsilon_{kl}} \right)_S \tag{2.13}$$

The adiabatic elastic constants are most relevant to elastic wave propagation where, in most situations, the time scale of deformation is much shorter than that of thermal diffusion over relevant length scales. Isothermal elastic constants are relevant, for example, in the analysis of static compression experiments [14]. In the limit of zero temperature and in the absence of zero-point motion, conditions corresponding to most first-principles theoretical calculations, adiabatic, and isothermal elastic constants are identical and are referred to as athermal elastic constants.

It is worth pointing out that other definitions of the elastic constants are possible [3]. In order to distinguish them, the c_{ijkl} are called the stress-strain coefficients. We may alternatively define

$$C^T_{ijkl} = \rho \left(\frac{\partial^2 A}{\partial \epsilon_{ij} \partial \epsilon_{kl}} \right)_T \tag{2.14}$$

which is identical to c_{ijkl} only in the absence of prestress. In the case of isotropic prestress — defined by $\sigma_{ij} = -P\delta_{ij}$ where P is the pressure — the two sets of elastic constants are related by [3]

$$C_{ijkl} = c_{ijkl} + P(\delta_{jl}\delta_{ik} + \delta_{il}\delta_{jk} - \delta_{ij}\delta_{kl}) \tag{2.15}$$

The C_{ijkl} do not relate stress to strain in general, and are not directly related to the velocity of elastic waves. They are however useful in defining the Cauchy relations (see below).

The wave propagation coefficients are [4]

$$A^S_{ijkl} = \rho \left(\frac{\partial^2 E}{\partial u_{ij} \partial u_{kl}} \right)_S \tag{2.16}$$

They are related to the stress-strain coefficients by

$$A_{ijkl} = c_{ijkl} + P(\delta_{il}\delta_{jk} - \delta_{ij}\delta_{kl}) \tag{2.17}$$

Because the deformation gradient u is not symmetric, A does not possess the full Voigt symmetry of the other elastic constants.

There are 81 independent stiffness coefficients in general; however, this number is reduced to 21 by the requirement of the Voigt symmetry that c_{ijkl} and C_{ijkl} are symmetric with respect to the interchanges (i, j), (k, l), and (ij, kl). This allows replacement of a pair of Cartesian indices ij by single index α, according to the scheme

$$\begin{aligned} ij &= 11 \;\; 22 \;\; 33 \;\; 32 \; or \; 23 \;\; 31 \; or \; 13 \;\; 21 \; or \; 12 \\ \alpha &= \;\; 1 \;\; 2 \;\; 3 \;\;\;\; 4 \;\;\;\;\;\; 5 \;\;\;\;\;\; 6 \end{aligned}$$

The diagonal constants c_{ii} with $i \leq 3$ may be referred to as the longitudinal elastic constants; c_{ii} with $i \geq 4$ may be called the shear elastic constants. Those c_{ij} with $i \neq j < 3$ are referred to as the off-diagonal constants and finally, c_{ij} with $i \leq 3$ and $j > 3$, which measure the shear strain produced by a longitudinal stress, may be called the mixed elastic constants.

The presence of the crystallographic symmetry further reduces the number of independent elastic constants [15]. The highest possible symmetry is that of an isotropic material such as a glass or a randomly oriented polycrystalline aggregate, which is fully characterized by two elastic constants. These can be defined as the bulk and shear modulus, K and G, respectively, or in terms of alternative moduli such as the Young's modulus or Lamé parameter, or ratios of moduli, such as the Poisson's ratio. Relationships among these measures are given in a number of sources [16]. A cubic crystal is characterized by three constants, C_{11}, C_{12}, and C_{44}. Crystals with lower symmetry will possess a larger number of independent constants, for example, 9 for orthorhombic crystals (C_{11}, C_{22}, C_{33}, C_{12}, C_{13}, C_{23}, C_{44}, C_{55}, and C_{66}), and 21 for triclinic crystals (the largest number possible).

Two applications illustrate the relationships among the various definitions of the elastic constants. The Cauchy relations are valid for a crystal in which each atom is located at a center of symmetry and whose atoms interact through central forces only. They are most naturally formulated in terms of the free energy-strain coefficients [2]

$$\begin{aligned} C_{12} &= C_{66}, C_{13} = C_{55}, C_{23} = C_{44} \\ C_{14} &= C_{56}, C_{25} = C_{46}, C_{36} = C_{45} \end{aligned} \tag{2.18}$$

But when defined in terms of the stress-strain coefficients (c_{ij}), the first three relations involve a pressure term, e.g., $C_{12} - C_{66} - 2P = 0$. The extent to which these conditions are violated represents the importance of noncentral forces in a crystal.

The Born stability criteria, which define the mechanical stability of a lattice, are typically formulated in terms of the C_{ijkl}. In this case, they are valid only in the limit of vanishing prestress. Several studies [17, 53] have demonstrated that the appropriate stability criteria for a stressed lattice are those which are formulated in terms of the stress-strain coefficients (c_{ijkl}) and hence are based on enthalpy considerations. Under hydrostatic pressure, the three stability criteria for a cubic crystal are

$$C_{11} + 2c_{12} > 0, C_{44} > 0, C_{11} - C_{12} > 0 \tag{2.19}$$

which are referred to as spinodal, shear, and Born criteria, respectively. The spinodal criterion is equivalent to requiring that the bulk modulus be positive.

2.2.3. Elastic Wave Velocities

The wave propagation coefficients (A_{ijkl}) appear in the equations of motion and hence determine the acoustic velocities [4]. For small vibrations to first order in the displacements u_i about the prestressed state, we can write

$$\rho \frac{\partial^2 u_i}{\partial t^2} = A_{ijkl} \frac{\partial^2 u_k}{\partial x_j \partial x_l} \tag{2.20}$$

The velocity (V) and polarization of the three waves along a given unit-propagation direction, n, are determined by the condition

$$|A_{ijkl} n_j n_l - \rho V^2 \delta_{ik}| = 0 \tag{2.21}$$

In the special case of hydrostatic prestress, the wave propagation coefficients may be replaced by the stress-strain coefficients as follows: because of the sum over j and l only the symmetric combination

$$A_{ijkl} + A_{ilkj} = c_{ijkl} + c_{ilkj} \tag{2.22}$$

appears where the identity follows from Eq. 2.17. The velocities are then given by

$$|c_{ijkl} n_j n_l - \rho V^2 \delta_{ik}| = 0 \tag{2.23}$$

which is known as the Christoffel equation [2]. The equation shows that under a condition of hydrostatic prestress the stress-strain coefficients govern elastic wave propagation.

The solutions are of two types: a quasi-longitudinal wave with polarization nearly parallel to the direction of propagation, and two quasi-shear waves with polarization nearly perpendicular to n. In seismology, the quasi-longitudinal wave is usually referred to as the P-wave (i.e., primary, or first to arrive at the recording station from the earthquake) and the quasi-shear waves as S-waves (secondary). Pure longitudinal and shear polarizations are found only in isotropic materials or along special high-symmetry propagation directions in anisotropic materials. For an isotropic, homogeneous material, the P- and S-wave velocities are related to the elastic moduli by

$$V_P = \sqrt{\frac{K + \frac{4}{3}G}{\rho}}; \quad V_S = \sqrt{\frac{G}{\rho}} \tag{2.24}$$

from which the bulk sound velocity

$$V_B = \sqrt{\frac{K}{\rho}} = \sqrt{V_P^2 - \frac{4}{3}V_S^2}. \tag{2.25}$$

can also be defined.

Because the elastic constant tensor is fourth-ranked, all crystals are elastically anisotropic regardless of symmetry. One consequence is that the elastic wave velocities depend on the direction of propagation. Two types of velocity anisotropy may be considered. Azimuthal anisotropy refers to the dependence of the elastic wave velocity on the propagation direction. Polarization anisotropy is relevant only to shear waves and describes the dependence of velocity on polarization along a single propagation direction. For cubic crystals, azimuthal and maximum polarization anisotropy are determined by a single anisotropy factor [17]

$$A = \frac{2c_{44} + C_{12}}{c_{11}} - 1 = \frac{2(C_{44} - c_s)}{C_{11}} \tag{2.26}$$

where $c_s = (C_{11} - C_{12})/2$.

2.2.4. Polycrystalline Aggregates

If the length scale of deformation (e.g., the wavelength of the elastic wave) is much larger than the grain size, then the response of the material is that of an aggregate. The elastic properties of an aggregate can be uniquely calculated from the single crystal elastic constants if the texture can be specified, that is, the positions, shapes, and orientations of the grains. The texture is typically unknown, or difficult to characterize completely. A special case is an isotropic monophase aggregate in which the grains are assumed to be randomly oriented but the texture is left otherwise unspecified. Because the texture is only partially known, determination of the elastic moduli is inherently nonunique. Nevertheless, it is possible to construct rigorous bounds. The most commonly used are the Voigt and Ruess bounds which correspond to a condition of, respectively, strain and stress continuity across grain boundaries [18, 19]. The Hashin–Shtrikman [20] bounds are tighter. In the case of cubic crystals, the bulk modulus is uniquely defined by

$$K = \tfrac{1}{3}(C_{11} + 2c_{12}) \tag{2.27}$$

The isotropic shear modulus in the Hashin–Shtrikman averaging scheme is given by

$$G_{HSA} = \tfrac{1}{2}(G_{HS_+} + G_{HS-}) \tag{2.28}$$

where the upper and lower bounds (interchangeable) are

$$G_{HS+} = C_{44} + 2\left(\frac{5}{c_s - C_{44}} + \frac{18(K + 2c_{44})}{5c_{44}(3K + 4c_{44})}\right) \tag{2.29}$$

and

$$G_{HS-} = c_s + 3\left(\frac{5}{C_{44} - c_s} + \frac{12(K + 2c_s)}{5c_s(3K + 4c_s)}\right) \tag{2.30}$$

respectively. Formulas for lower symmetry crystals have been derived; see [21] for a review.

Bulk anisotropy of monophase aggregates may be caused by lattice-preferred orientation (LPO) of the grains. LPO may develop, for example, under shear deformation because of crystallographically preferred directions of dislocation glide. The anisotropy of the aggregate can be no larger than that of the constituent single crystals; often it is a factor of two to three smaller than that of the single crystal depending on the degree of alignment and the details of the texture. Polyphase aggregates may exhibit LPO or a different type of anisotropy due to shape-preferred orientation (SPO). In SPO, the anisotropy is due to spatial inhomogeneity in the distribution of phases [22] as in a laminated structure, for example.

For monophase aggregates, or for polyphase aggregates in which the spatial distribution of the phases is random, the elastic constants of the aggregate, c'_{ijkl} can be related to the single crystal elastic constants, c_{ijkl} by

$$c'_{ijkl} = \sum_{agg} a_{im} a_{jn} a_{ko} a_{lp} f(\theta) c_{mnop} \tag{2.31}$$

where the elements of the coordinate transformation matrix a_{ij} are the direction cosines of the angles that relate crystallographic and laboratory coordinate systems, and f is the orientation distribution function (ODF) which yields the probability of finding a crystal with orientation specified by θ [23].

2.2.5. Microscopic Basis

The microscopic understanding of the elastic constants is based on an analysis of the total energy (also called the crystal potential). The elastic constants can be calculated from the crystal potential in one of two ways: the method of homogeneous deformation and the method of long waves [1].

In the method of homogeneous deformation, the derivatives of the total energy with respect to a uniform strain are computed. In most calculations of the elastic constants based on density functional theory or other band structure methods, a small but finite strain is applied to the crystal and the total energy and its derivatives (e.g., the stress tensor) are recomputed in the strained configuration. Consider a homogeneous deformation, u_{ij}, applied to a crystal with one or more atoms in the unit cell. The resulting displacement of atom α in unit cell L can be written [4]

$$U_i(L, \alpha) = S_i(\alpha) + u_{ij} R_j(L, \alpha) \tag{2.32}$$

where R_j is the position of the atom, and S_i are the sublattice displacements. The displacement gradients are the independent variables, and the sublattice displacements must be regarded as being dependent upon them. The presence of sublattice displacements, which has been described as arising from coupling between lattice strain and optic vibrational modes in crystals, has important consequences for the computation of the elastic constants by the method of homogeneous deformation; the equilibrium positions of the atoms must be redetermined in the strained configuration. The effect of sublattice displacements on the elastic constants may be very large as discussed in the following paragraphs. In order to illustrate the influence of structural relaxation, it is possible to calculate separately those contributions to the elastic constants arising from the homogeneous deformation in the absence of structural relaxation, also called the partial elastic constants, and those from the sublattice displacements, also called the inner elastic constants [24].

The method of long waves is based on the equivalence of compressional and shear elastic waves and long-wavelength longitudinal and transverse acoustic phonons, respectively. The long-wavelength acoustic phonon velocity, c, in direction k is given by the dispersion relation in the limit of small wavevector

$$\omega_s(k) = c(\hat{k})|k| \tag{2.33}$$

where ω is the frequency, s is the branch index that runs over the acoustic phonons, and $\hat{k}$ is a unit vector in the direction of k. The velocities are the eigenvalues of

$$d_{ik}(\hat{k}) = \frac{1}{\rho} \sum_{jl} \hat{A}_{ijkl} \hat{k}_j \hat{k}_l \tag{2.34}$$

where $\hat{A}$ is similar to A, but defined in terms of the crystal potential rather than the thermodynamic internal or free energy. In the limit of the static lattice, or more

generally, when the potential energy of the crystal is much larger than the kinetic energy, $\hat{A}$ may be replaced by A and the phonon velocities are identical with the elastic wave velocities

$$c(\hat{k}) = V(\hat{k}) \tag{2.35}$$

Wallace discusses the relationship between the acoustic phonon velocities in the more general case of finite temperatures [4].

2.2.6. Anelasticity

The response of materials to stress or strain is not in general perfectly elastic. Strain is time dependent in an anelastic material and the resulting strain-energy losses are expressed in terms of the quality factor Q

$$\frac{2\pi}{Q} = -\frac{\Delta E}{E} \tag{2.36}$$

The quality factor may be a strong function of frequency. Over the range of frequencies probed in the laboratory ($\sim$ GHz for Brillouin scattering and $\sim$ MHz for ultrasonic measurements), anelasticity does not usually affect measurements of elastic constants of crystals. At the much lower frequencies probed by seismology, the earth is measurably anelastic; quality factors for shear waves range from >1000 in the lithosphere to $\sim$300–500 throughout much of the mantle [25]. Liquids commonly show attenuation at experimental frequencies [26]. Measurements of anelasticity typically show that attenuation in shear is much greater than that in volume compression. This is consistent with laboratory measurements of the equation of state of crystals by static compression (essentially zero frequency) which agree with the bulk modulus measured by high-frequency techniques. Anelasticity entails dispersion (frequency dependence) of elastic wave velocities; for a standard linear (Maxwell or viscoelastic) solid the fractional difference between velocities at zero and infinite frequency is $1/Q$.

2.2.7. Fluids

Except at very high frequencies, liquids cannot support shear deformation, and so the elasticity is completely specified by the bulk modulus (inverse of the compressibility). An important result in the study of simple liquids is the relationship between the structure and the elasticity. For a monatomic liquid [27]

$$S(0) = \rho k_B T / K_T \tag{2.37}$$

where the static structure factor $S(k)$ is evaluated in the long-wavelength limit, k_B is the Boltzmann constant, and K_T is the isothermal bulk modulus. This relationship may also be expressed in terms of the pair correlation function, $g(r)$, which is the probability of finding a pair of atoms separated by a distance, r. The pair correlation function is normalized so that it approaches unity (the ideal gas value) at large r. Recognizing that the structure factor is just the Fourier transform of the total correlation function $h(r) = g(r) - 1$

$$\rho k_B T / K_T = 1 + \rho \int [g(r) - 1] dr \tag{2.38}$$

Finally, defining the direct correlation function through the Ornstein–Zernicke equation

$$h(r) = c(r) + \rho \int c(|r - r'|) h(r' dr') \tag{2.39}$$

one can show that

$$\rho \hat{c}(0) = 1 - \rho k_B T / K_T \tag{2.40}$$

where $\hat{}$ denotes Fourier transform. The above relations are easily generalized to multicomponent homogeneous isotropic fluids. Other generalizations have also been widely studied, including the anisotropic case relevant to liquid crystals [28].

At very high frequencies, fluids are able to support shear deformation, and the shear modulus as well as the bulk modulus must be specified. The relevant time scale in the viscoelastic approximation is the Maxwell relaxation time

$$\tau_M = \frac{\eta}{G_\infty} \tag{2.41}$$

where η is the shear viscosity and G_∞ is the shear modulus of the fluid in the limit of infinite frequency. The Maxwell relaxation time of a liquid may become comparable to the period of typical experimental probes if the viscosity of the liquid is large, which may occur near the glass transition, for example. Many liquids, even above the melting point, have viscosities sufficiently large that the Maxwell relaxation time exceeds the period of typical ultrasonic probes — examples include silicate liquids that are representative of naturally occuring magmas [26].

It is worth noting that the converse of these arguments also holds. That is, if a solid is deformed at time scales much longer than its Maxwell relaxation time, it will flow. The Maxwell relaxation times of typical solids are very long and may exceed the age of the universe at ambient conditions. However, the viscosity of most solids is an exponentially decreasing function of temperature. In the earth's interior, where temperatures approach 90% of the melting point, the Maxwell relaxtion times of silicates may be as little as one thousand years. Over geologically significant periods of time, the earth's solid mantle behaves to a good approximation as a Newtonian viscous fluid, as manifested, for example, in mantle convection, postglacial rebound, and the shape of the earth [29].

2.3. THEORETICAL METHODS

2.3.1. First-Principles Level

Density functional theory [5, 6] has become a powerful tool for examining the elasticity of materials. Central to the theory is the proof that ground-state properties are a unique functional of the charge density; it is not necessary to solve for the complete 10^{23} dimensional total wavefunction. This is appealing because the charge density, a scalar function of position, is readily observable experimentally, e.g., by x-ray diffraction.

The Schödinger-like Kohn–Sham equations

$$\left[-\Delta^2 + V_{KS}\right] \psi_i = \epsilon_i \psi_i \tag{2.42}$$

where the Kohn–Sham potential

$$V_{KS}[\rho(\vec{r})] = \sum_{i=1}^{N} \frac{2Z_i}{|\vec{r} - \vec{R}_i|} + \int \frac{2\rho(\vec{r}')}{|\vec{r}' - \vec{r}'|} d\vec{r}' + V_{xc}[\rho(\vec{r}')] \tag{2.43}$$

(where Z_i and R_i are the nuclear charges and positions, respectively, and V_{xc} is the exchange-correlation potential), are solved self-consistently with the charge density, ρ. The Kohn–Sham equations are exact in principle. However, the exact form of the many-body exchange-correlation functional is not known. In practice, approximations to this term are adopted, the simplest being the local density approximation (LDA) which sets the exchange-correlation functional at every point in the crystal to that of the free-electron gas of the same charge density at that point [30]. The generalized gradient approximation (GGA) also depends on local charge density gradients [31]. Comparison with experiment has demonstrated that the LDA is a good approximation

for silicates and oxides, and most representatives of all other classes of materials. There is some evidence that the GGA may be more accurate in some cases for transition metals [32] and silicates [33].

It is possible to solve the Kohn–Sham equations without any further essential approximation beyond that to the exchange-correlation functional. For example, the linearized augmented plane wave (LAPW) includes all electrons and contains no uncontrolled approximations to the shape of the charge density or potential [34, 35]. The LAPW method has been applied to systems containing as many as 20 atoms in the unit cell [36]. However, the method is relatively slow and still prohibitive for many of the large and complex structures important in many fields including geophysics and materials science.

An alternative method that is much more efficient, though at the cost of additional approximations, is the plane-wave pseudo-potential method. The development is based on the observation that over the range of conditions normally encountered only the valence electrons are altered by changes in state of stress or temperature; the core electrons are essentially static or frozen. The nucleus and core electrons are then replaced by a simpler object, the pseudo-potential, which has the same scattering properties [37]. This is computationally advantageous because the pseudo-potential is much softer (much more slowly varying in space) than the bare Coulomb potential of the nucleus. Moreover, one need solve self-consistently only for the valence electrons which also show much more gentle spatial variations. As a result, the charge density and potential may be represented by a set of plane waves of manageable size, speeding the calculation by perhaps an order of magnitude compared with the LAPW method. Calculations show that as long as the quality of the pseudo-potential is carefully evaluated by comparison with limited all electron calculations, the pseudo-potential approximation is generally not serious in the case of silicates and oxides.

2.3.1.1. Static Lattice

Given an arrangement of nuclei, density functional theory allows one to calculate the resulting electronic charge density and total energy. By examining the variations in the total energy with respect to displacements of the nuclei or strains applied to the structure, one makes contact with a number of experimentally observable quantities. For example, by differentiating the relationship between total energy and volume, one obtains the static equation of state. The full elastic constant tensor can be calculated by examining the variation of the total energy with respect to small applied strains [38].

The scope of density functional calculations has been substantially expanded with the development of first-principles molecular dynamics [9, 10]. This development is based on the Hellman–Feynman theorem which says that it is possible to calculate directly the forces acting on the nuclei and the stresses acting on the lattice. This is important for at least two related reasons. It allows one to determine efficiently and accurately: (1) equilibrium structures which, at a given volume or pressure, are found by systematically adjusting the positions of the nuclei and the lattice parameters until forces and deviatoric stresses vanish (e.g., by steepest descent) making it then possible to examine the compression of complex crystal structures, and to study structural compression mechanisms in detail; and (2) elastic constants. Once the equilibrium structure has been determined, the elastic constants are calculated in a way that mimics experimental methods. A small deviatoric strain is applied to the lattice and the resulting stresses calculated. The ratio of stress to strain components yields a subset of the elastic constants of the material. By applying a small set of strains of different symmetry it is possible to obtain the full elastic constant tensor. Because elastic constants generally couple to vibrational modes in complex structures such as those of silicates, it is important to redetermine the equilibrium arrangement of the nuclei in each strained configuration.

2.3.1.2. Finite Temperature

The static lattice is an athermal idealization that is not accessible experimentally: temperature is absent, and so is zero-point motion. For many materials at room temperature, the effect of zero-point motion and temperature on material properties and crystal structures is small, often smaller than the effect of the LDA or GGA approximations. As a result, comparison of static calculations to room-temperature experimental measurement can yield considerable insight.

The generalization of the first-principles methods described so far to the calculation of properties at finite temperature is straightforward but computationally challenging. We must deal explicitly with the dynamics of the atomic motions to account for high temperature behavior. This may be accomplished through molecular dynamics simulations, which have been used to compute elastic constants in simple systems that are represented by pair potentials. High-temperature elastic constants may also be determined by computing the phonon dispersion curve and its strain derivatives. This procedure has successfully been carried out at the level of density functional theory for MgO [39].

2.3.2. Ab Initio Level

Whereas first-principles methods seek to reduce approximations to a bare minimum, ab initio methods construct an approximate model of some aspects of the relevant physics, such as the charge density or the interactions between orbitals. The cost of additional approximation is often outweighed by the increase in computational simplicity and efficiency. For example, ab initio models have been used to explore transport properties which are very difficult (costly) to examine with fully first-principles approaches [40]. Moreover, these models often yield insight that is sometimes difficult to extract from more complex and elaborate first-principles calculations.

Here are two examples of ab initio methods that have been applied to the calculation of elastic constants. First, are those methods based on the electron gas picture of Gordon and Kim [41] in which the material is viewed as being composed of spherically symmetric closed-shell ions. Modern elaborations of this approach that account for the deformability of the ions, including the potential induced breathing model (PIB) and the variationally induced breathing (VIB) model have enjoyed wide success, especially as applied to simple oxides such as MgO [42, 43]. Second, are the parametric total energy tight binding methods [44]. Here the interactions between atomic-like orbitals are approximated by simple functional forms that are made to fit accurate first-principles total energy and band-structure results. One recent method of this type has successfully been used to examine the elasticity of monatomic transition metals, insulators, and semiconductors [45, 46].

2.3.3. Semi-Empirical Level

Semi-empirical methods differ from those discussed so far in that they require input from experiment. These methods often do not view the solid as being composed of nuclei and electrons, but of larger entities. Interatomic force models view the solid as being composed of atoms or ions that interact as a unit with their neighbors. Models of this type have been widely used to study elasticity [1]. They are generally less predictive than first-principles or ab initio calculations because they ignore much of the essential physics. For example, a pair-wise central interatomic force model exactly satisfies the Cauchy relations (Eq. 2.18) in disagreement with observations on many materials. The primary advantage of interatomic force models is that they are simple and rapid. They are useful to the extent that they faithfully interpolate or extrapolate existing experimental or theoretical results or provide additional insight not otherwise available.

2.3.4. Continuum Theories

Another broad class of semi-empirical methods is based on a continuum picture in which one deals with material behavior at the macroscopic level of thermodynamics. An important example is the Eulerian finite strain theory of Birch [47] which has been widely used in the extrapolation of the equation of state to high pressure. In the case of isotropic properties, this theory has been demonstrated to converge rapidly in most cases. Here we review the generalization of this approach to anisotropic strains, which has not been widely studied [11].

The strain corresponding to the hydrostatic prestress will be finite in general. We will assume that this finite strain is isotropic, recognizing that this will only be valid for materials of cubic or higher symmetry. Of the infinite number of (reference-frame dependent) possible choices for the finite isotropic strain tensor, we choose the Eulerian strain. The trace is

$$f = \tfrac{1}{2}[(V/V_0)^{-2/3} - 1] \tag{2.44}$$

where V is the volume, subscript 0 indicates the reference state, and we have defined f positive on compression. The dependence of the internal energy on finite strain may be described by a Taylor series

$$E = a_0 + \tfrac{1}{2}a_2 f^2 + \tfrac{1}{3}a_3 f^3 + \cdots \tag{2.45}$$

where the coefficients a_n involve nth and lower-strain derivatives of E evaluated at the reference state, e.g., the internal, pressure, the bulk modulus.

The finite-strain expansion for the adiabatic elastic constants is found by evaluating the appropriate derivatives of the internal energy with respect to the deviatoric strains

$$c_{ijkl}(f, T) = (1 + 2f)^{7/2}(R^{(0)}_{ijkl} + R^{(1)}_{ijkl} f + \tfrac{1}{2}R^{(2)}_{ijkl} f^2 + \cdots) - P\Delta_{ijkl} \tag{2.46}$$

where

$$R^{(0)}_{ijkl} = c_{ijkl0} + P_0\Delta_{ijkl} \tag{2.47}$$

$$R^{(1)}_{ijkl} = 3K_0(c'_{ijkl0} + \Delta_{ijkl}) - 7R^{(0)}_{ijkl} \tag{2.48}$$

$$R^{(2)}_{ijkl} = 9K_0^2 c''_{ijkl0} + 3K'_0(R^{(1)}_{ijkl} + 7R^{(0)}_{ijkl}) - 16R^{(1)}_{ijkl} - 49R^{(0)}_{ijkl} \tag{2.49}$$

where primes indicate pressure derivatives,

$$\Delta_{ijkl} = -\delta_{ik}\delta_{jl} - \delta_{il}\delta_{jk} - \delta_{ij}\delta_{kl} \tag{2.50}$$

and δ_{ij} is the Kroenecker delta tensor. Because we have defined f as positive on compression, the coefficients in the Taylor series expansion are related to those of [11] by $R^{(n)}_{ijkl} = (-1)^n \rho_0 r^{(n)}_{ijkl}$, where ρ is the density.

The reference state, in which $f = 0$ and T is the temperature of interest is indicated by subscript 0. Here, we will choose our reference state to be one of constant pressure, $P_0 = 0$. In this case, reference state quantities, including the coefficients of the expansion, $R^{(n)}$ depend on temperature in general.

The effects of temperature are included within the quasi-harmonic approximation. The strain dependence of the vibrational frequencies, ω_ν, where the subscript absorbs the wavevector and branch index, may be described by an expansion in the strain

$$\omega_\nu^2 = \omega_{\nu 0}^2 \left(1 - g^\nu_{ij} f_{ij} + \tfrac{1}{2}h^\nu_{ijkl} f_{ij} f_{kl} + \cdots\right) \tag{2.51}$$

where g^ν_{ij} and h^ν_{ijkl} are constants that will in general be different for each mode and so will depend on wavevector and frequency. In what follows, we assume that these constants can be replaced by appropriate averages over all the modes, g_{ij} and h_{ijkl}.

In this approximation, the elastic moduli at high temperature are given by Eq. 2.46 with

$$R^{(0)}_{ijkl} = c_{ijkl00} + \tfrac{1}{4}(2h_{ijkl} - g_{ij}g_{kl})\cdot[E_{TH0}(T) - E_{TH0}(T_0)]/V_0 \tag{2.52}$$

and $R^{(n)}$ for $n > 0$ evaluated at the reference strain and reference temperature $T = T_0$. Subscript 00 indicates values at the reference strain and temperature $T = T_0$, and E_{TH} is the quasi-harmonic thermal energy. By explicitly accounting for the temperature dependence of only the first expansion coefficient, we introduce errors of order $\delta^2 f$ where δ is the relative magnitude of the anharmonic contributions to the crystal Hamiltonian [11]. The parameters g and h are evaluated by relating them to thermodynamic quantities. For the special case of a cubic material

$$g_{ij} = -2\gamma_0\delta_{ij} \tag{2.53}$$

where γ is the Grüneisen parameter,

$$\gamma = \frac{K_T\alpha V}{C_V} \tag{2.54}$$

and

$$h_{ijkl} = -2\gamma_0\left[\xi_0\delta_{ij}\delta_{kl} + \delta^T_{ijkl0} - \left(\frac{\partial c^T_{ijkl}}{\partial P}\right)_0\right] + 4\gamma_0^2\delta_{ij}\delta_{kl} - 2\gamma_0\delta_{ik}\delta_{jl} - 2\gamma_0\delta_{jk}\delta_{il} \tag{2.55}$$

where

$$\xi = 1 - \left(\frac{\partial ln Cv}{\partial ln V}\right)_T \tag{2.56}$$

$$\delta^T_{ijkl} = -\frac{1}{\alpha K_T}\left(\frac{\partial c^T_{ijkl}}{\partial T}\right)_P \tag{2.57}$$

where c^T_{ijkl} are the isothermal elastic moduli, and C_V is the heat capacity at constant volume. These expressions have been used to examine the elasticity of MgO at elevated temperature and pressure [48].

2.4. ELASTICITY OF SOLIDS

2.4.1. Oxides and Elements

2.4.1.1. Atomistic Origin of Anisotropy

The origin of elastic anisotropy is most easily seen by considering a simplified situation in which the material is monatomic and the atoms interact through central nearest-neighbor forces (CNNF). The CNNF model has been widely studied [1] in the context of elasticity. If the crystal has no sublattice displacements under deformation, and all nearest-neighbor distances are the same, the elastic constants (energy-strain coefficients) are

$$C_{ijkl} = \frac{9}{z}(K - P)\sum_\alpha \hat{r}^\alpha_i\hat{r}^\alpha_j\hat{r}^\alpha_k\hat{r}^\alpha_l \tag{2.58}$$

where z is the coordination number, K the bulk modulus, P the pressure, and the sum runs over the nearest neighbors, α, which are located along the unit directions $\hat{r}$. If sublattice displacements do occur, then this expression yields the partial elastic constants. For the CNNF model, elastic constants are independent of the form of the

interatomic force. The stress-strain coefficients contain an additional term involving the pressure, and so will depend on the form of the potential; however, the dependence is not strong, being of the order P/C_{11} [46].

For the fcc structure, CNNF yields elastic constants in the proportions

$$C_{11} : C_{12} : C_{44} = 2 : 1 : 1 \tag{2.59}$$

where the equality of C_{12} and C_{44} also follows from the Cauchy condition. Similar results have been derived for the hcp structure; the bcc and sc structures are elastically unstable in the CNNF approximation. The anisotropy factor for the fcc structure $A = 1/2$, and corresponds to a large P- and S-wave velocity anisotropy. This is an important result because it shows that elastic anisotropy may arise from geometry alone, that is, from the anisotropic distribution of neighbors in the crystal structure. The CNNF model, despite its simplicity, approximates the behavior of a wide range of monatomic materials at high pressure including fcc and hcp structures of Fe, Si, and Xe [46], and the hcp transition metals, except for Zn and Cd [38].

In many cases, it is possible to rationalize in a simple way the effect of crystallographic structure on the elasticity of materials. An example is the large P-wave anisotropy in the mineral forsterite (Mg_2SiO_4) (Fig. 2.1). The orthorhombic structure is composed of two types of coordination polyhedra: SiO_4 tetrahedra which are relatively incompressible, and comparatively soft MgO_6 octahedra. The polyhedral bulk moduli of tetrahedra and octahedra differ by approximately a factor of three [49]. A view of the forsterite structure down the b-axis shows that perpendicular to the a-axis (that of fastest P-wave propagation) strips of SiO_4 tetrahedra alternate with strips of MgO_6 octahedra (Fig. 2.2). The anisotropy results from: (1) the inherent anisotropy of the structure; and (2) the very different compressibilities of its two primary polyhedral elements. Longitudinal waves propagating parallel to these strips (along c), will be primarily sensitive to the easily deformable MgO_6 octahedra and therefore slow. Waves propagating along a, however, will be sensitive to the compressibility of both tetrahedra and octahedra and are much faster as a result.

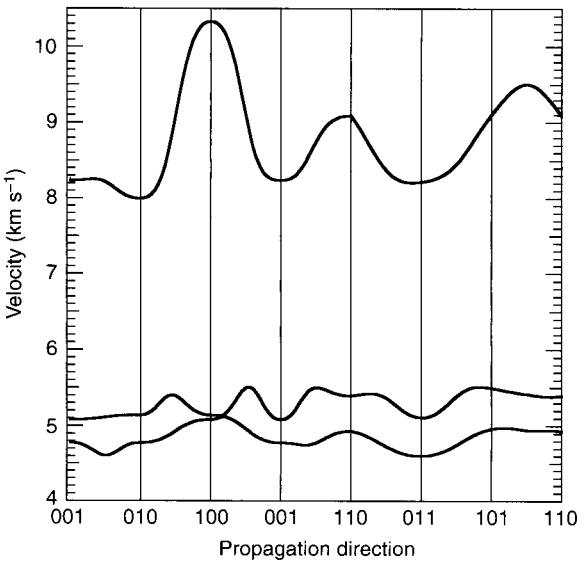

Fig. 2.1. Anisotropy of forsterite showing the P-wave (upper line) and S-wave (lower lines) velocities as a function of propagation direction; from the LDA pseudo-potential calculations of [65].

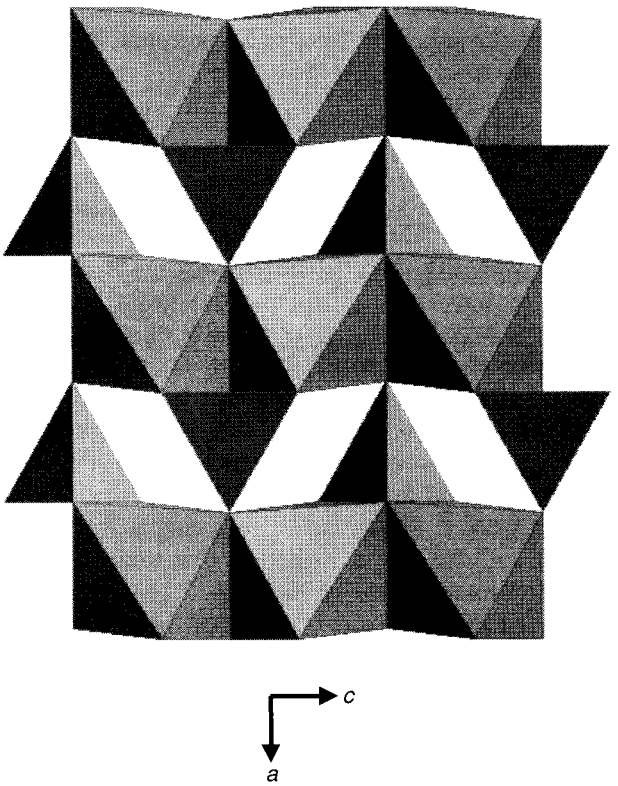

Fig. 2.2. Structure of forsterite looking down the *b*-axis showing alternating strips of Mg-octahedra (lighter polyhedra) and Si-tetrahedra (darker).

2.4.1.2. Cauchy Violations

The Cauchy conditions are satisfied closely for some materials (e.g., the alkali halides) indicating that the atoms in these solids interact dominantly through central forces. This is not surprising because of the large energetic contribution of the Madelung term. However, other ionic materials behave differently. For example, MgO and CaO, both of which have the NaCl structure at low pressure, violate the Cauchy conditions; $C_{12} - C_{44} - 2P$ at ambient pressure is 30% of the bulk modulus. Cubic perovskite-structure $CaSiO_3$ is an example of a silicate that violates the Cauchy conditions. Moreover, the magnitude of the violation in oxides and silicate increases with increasing pressure (Fig. 2.3). The strong violation of the Cauchy conditions in these materials requires an important contribution from noncentral (many-body) forces which increases with pressure. The noncentral forces can neither be due to metallic binding — since all the materials studied remain wide-gap insulators over the relevant pressure range [50] — nor to covalent forces in these ionic materials. The potential-induced breathing model includes the essential physics [51]. The relevant many-body force arises from a spherically symmetric breathing of the oxygen ion in response to strain-induced variations in the Madelung potential at the oxygen site.

2.4.1.3. Strong Coupling to Vibrational Modes

Sublattice displacements can have a large effect on the elastic constants. The effects of the coupling are particularly large in the presence of soft vibrational modes, as shown by the case of silica [52, 53]. In the stishovite (rutile-structured) phase, a soft

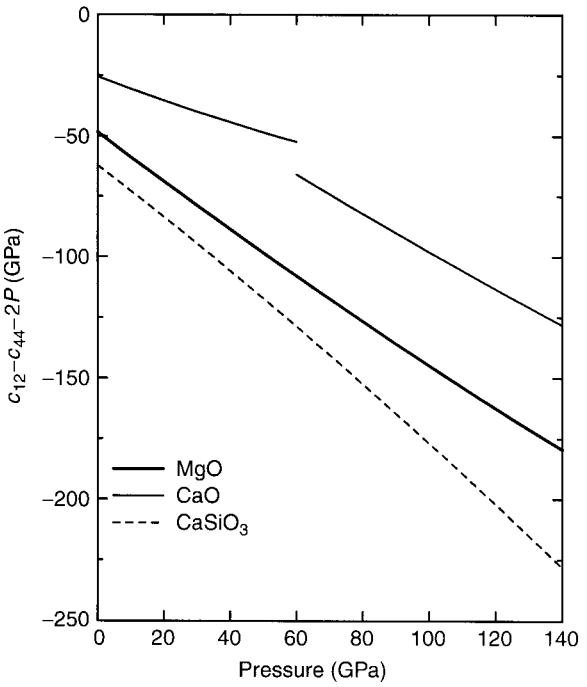

Fig. 2.3. Violation of the Cauchy relations in three materials according to density functional theory calculations (pseudo-potential calculations within LDA). From [60].

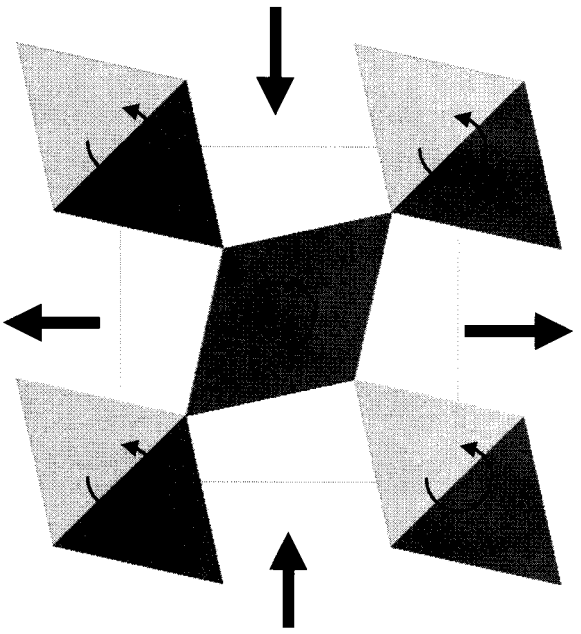

Fig. 2.4. Structure of stishovite looking down the c-axis showing the rotations of the octahedra in the soft B_{1g} Raman mode, and the shear strain in the $a = b$ plane to which they couple.

B_{1g} Raman mode couples strongly with a strain of orthorhombic symmetry in the $a = b$ plane (Fig. 2.4). The Raman mode consists of a rotation of the SiO_6 octahedra about the c-axis. As a result, the elastic constants $C_{11} - C_{12}$ is 30% smaller at ambient pressure than the corresponding partial elastic constant which neglects the sublattice displacements.

2.4.2. Transition Metals

2.4.2.1. Effect of D-band Filling

The variation of many physical properties across the transition metal series can be understood in terms of filling of a rigid d-band. Of the elastic constants, the bulk modulus is most amenable to this type of analysis, which we illustrate here following [54]. The bonding energy is assumed to arise from a d-band of rectangular form (Friedel model)

$$E_{bond} = 2\int_{\epsilon d - W/2}^{E_F} (E - \epsilon_d)\frac{5}{W}dE = -\frac{W}{20}N(10 - N) \tag{2.60}$$

where the band of width W is centered at ϵ_d, and E_F is the Fermi energy; the factor of five is the number of states in the band. The bonding energy is seen to vary quadratically with the number of d electrons closely mimicking trends observed in the cohesive energy. In equilibrium, the bonding energy must be balanced by a short-range repulsive energy, E_{rep}, among electrons on neighboring atoms, so that the cohesive energy

$$E_{coh} = E_{bond} + E_{rep} \tag{2.61}$$

The bandwidth will vary with compression as the average d-d hopping integral, and may be assumed, for fixed coordination number to have the form [55]

$$W = BNR^{-5} \tag{2.62}$$

The short-range repulsion, because it involves the repulsive overlap between two d-orbitals, may be expected to go as the square of the hopping integral

$$E_{rep} = AN^2R^{-10} \tag{2.63}$$

The bulk modulus is found by taking the appropriate volume derivatives of the energy

$$K_0 = \frac{50\sqrt{2}E_0}{9R_0^3} \tag{2.64}$$

where the cohesive energy in equilibrium is

$$E_0 = -\frac{1}{1600}\frac{B^2}{A}[N(10 - N)]^2 \tag{2.65}$$

and the equilibrium interatomic distance

$$R_0 = \left(\frac{40A}{B(10 - N)}\right)^{1/5} \tag{2.66}$$

and we have assumed an fcc lattice. We have determined the constants of proportionality A and B by fitting to first-principles results of the bandwidth and interatomic distance of fcc Mo ($N = 5$). We see that the trend of the bulk modulus across the 4d series is described qualitatively by this simple model (Fig. 2.5). It is possible to obtain better agreement with experiment by constructing a more elaborate form for the repulsive energy [54].

While the Friedel model succeeds in explaining most of the variation in the bulk modulus with d-band filling, it fails in the case of the shear elastic constants c_s and C_{44}. These two moduli are much more sensitive to the details of the electronic band structure [56]. Two patterns emerge in comparisons of accurate calculations with those based on the second-moment approximation. First, the second-moment approximation underestimates the dependence of the shear elastic constants on d-band filling; the actual

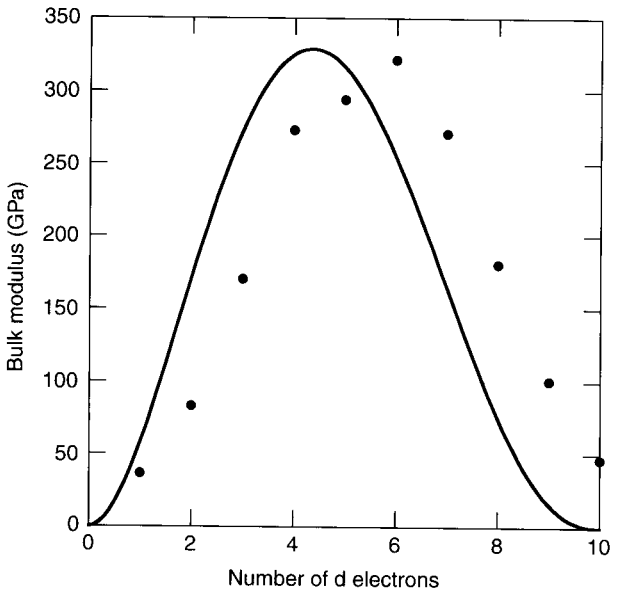

Fig. 2.5. Bulk modulus of the 4d transition metals (symbols) compared with the prediction of the second-moment Friedel model (line). All 4d transition metals are included regardless of structure because differences among structures are small compared with the effects of d-band filling.

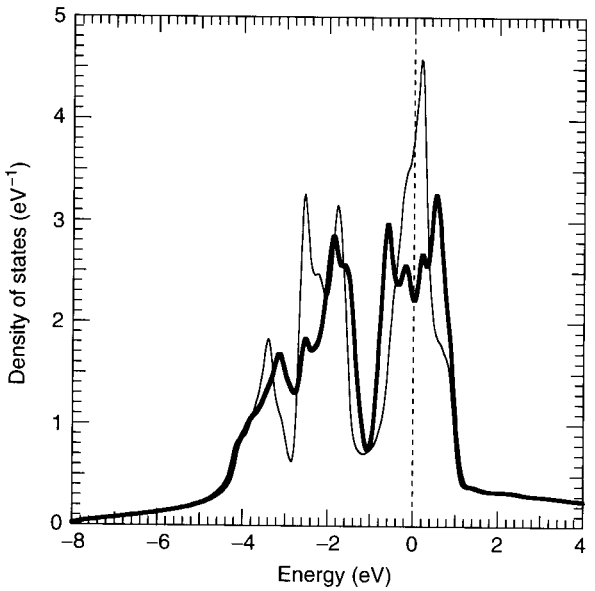

Fig. 2.6. Electronic density of states in (light) bcc iron and (bold) upon application of a tetragonal strain with $c/a = 1.2$. Dashed line is the Fermi energy.

elastic constants are 50% larger than the second-moment result near Ru. Second, sharp minima in the moduli are seen as a function of d-band filling that are absent in the more approximate calculations. These sharp minima arise from strain-splitting effects when the Fermi energy lies near narrow peaks or Van Hove singularities in the density of states.

The case of bcc iron illustrates the importance of strain splitting effects (Fig. 2.6). In the nonmagnetic state, the Fermi energy is coincident with a sharp peak. When the lattice is stretched along the cubic axis (corresponding to c_s), this peak is split and

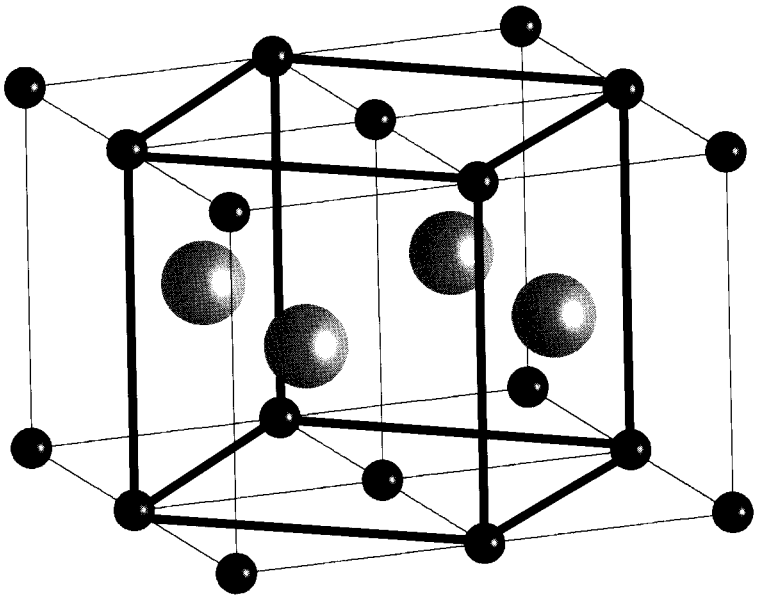

Fig. 2.7. Structure of cubic iron showing the Bains path that relates the bcc to the fcc structures. Light lines indicate four body-centered unit cells, bold lines the fcc conventional cell. Larger atoms are at body-centered positions in the bcc structure and face-centered positions in the fcc structure.

the band energy is lowered. As a result, nonmagnetic bcc iron is elastically unstable, with a negative value of c_s, violating the Born stability criterion. The stretch along the cubic axis relates the bcc structure to the fcc structure (Bains path) (Fig. 2.7). For the fcc structure, the form of the electronic density is such that strain-splitting effects are absent, and the structure is mechanically stable.

2.4.2.2. Role of Magnetism

Magnetism may have a large influence on the elastic constants. This is particularly true of materials such as bcc iron that are elastically unstable in the nonmagnetic state. The bcc phase of iron is stabilized by magnetism. This can be understood in a Stoner model: the up and down spin bands are viewed as being rigidly shifted in energy. As a result, the Fermi energy falls in between the narrow peaks in the density of states for up and down spin bands. Strain-splitting effects are absent in the magnetic state and the structure is stable at low pressure (Fig. 2.8).

At high pressure, the picture changes [57] (Fig. 2.8). The bands broaden and magnetism becomes increasingly less favorable energetically. The magnetic moment drops with increasing pressure, vanishing at a volume approximately 60% of the equilibrium value [58]. At this point, the mechanical instability of the underlying nonmagnetic state is revealed. The bcc phase of iron becomes mechanically unstable at high pressure. This is important in geophysics because it places some constraints on the crystalline structure of iron in the earth's inner core; it is unlikely to be bcc, as had frequently been proposed.

2.4.3. Effect of Pressure

2.4.3.1. Elastic Constants

The effect of pressure is much larger for certain types of elastic constants than for others: the pressure-induced variations in the longitudinal elastic constants are relatively

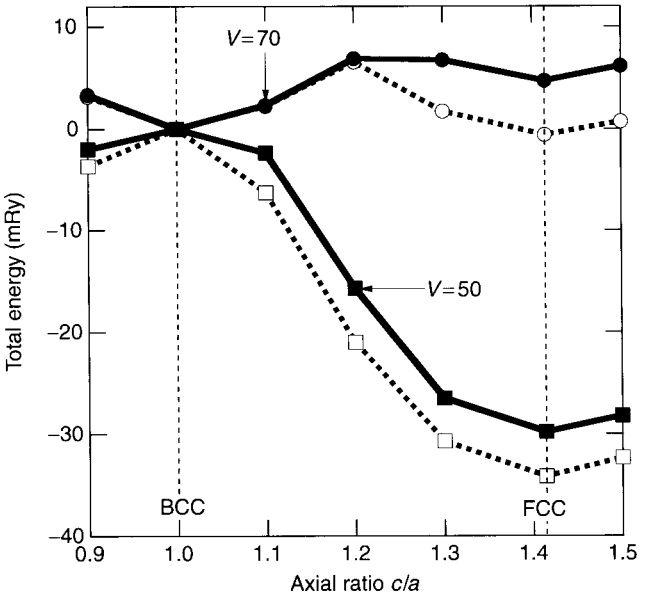

Fig. 2.8. Change in total energy of cubic iron along the Bains path according to spin-polarized density functional theory calculations (LAPW). Results at two different volumes are indicated corresponding to near ambient pressure (circles, $V = 70\text{Bohr}^3$), and high pressure (squares, $V = 50\text{Bohr}^3$, $P \approx 200$ GPa). Bold lines are in GGA, dashed lines in LDA. Axial ratios $c/a = 1$ corresponding to the bcc structure and $c/a = \sqrt{2}$ to the fcc structure are indicated. From [58].

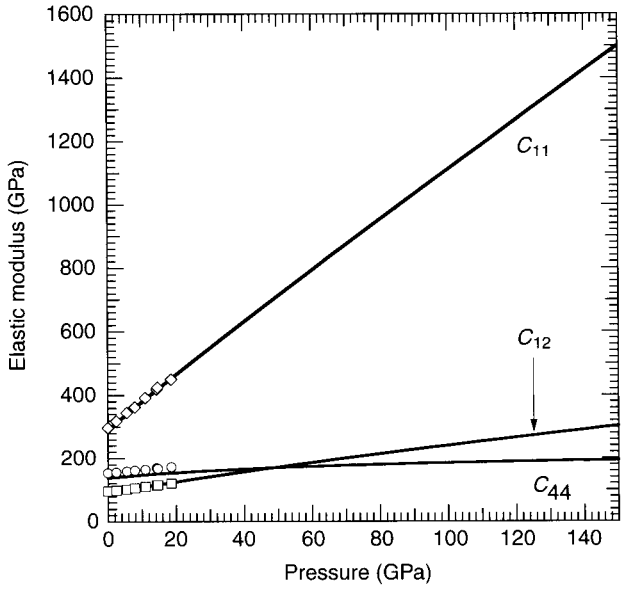

Fig. 2.9. Elastic constants of MgO according to LDA pseudo-potential calculations [17] and experiment [63].

large ($c'_{ij0} = 5$ to 10), compared to those for the shear and off-diagonal constants ($c'_{ij0} =$ 0.5 to 4); mixed elastic constants have the smallest pressure derivatives. The elastic constants of periclase are an example (Fig. 2.9). Finite-strain theory [16, 47] [11] can be used to understand the range of values of c'_{ij0} that are found for longitudinal, off-diagonal, and shear elastic constants. Expansions in the Eulerian finite strain are known

to provide rapidly convergent descriptions of isothermal compression (P-V equation of state), in some cases to compressions as great as $V_0/V = 2$. This success can be understood by recognizing that the coefficients of higher order terms are small [59]. For example, the truncation of the equation of state after second order (i.e., setting $a_3 = 0$ in Eq. 2.45) yields $K_0' = 4$, in good agreement with the range of values observed experimentally (typically 3–6). This implies that the coefficient a_3 should be small and that the third-order Birch–Murnaghan equation should be adequate for most materials. Truncation at the second order of the anisotropic generalization of the Eulerian finite-strain expansion ($R^{(1)}$ in Eq. 2.25) leads to the following relation for the pressure derivatives of the elastic constants:

$$c'_{ij0} = \frac{7}{3}\frac{c_{ij0}}{K_0} - \Delta_{ij} \tag{2.67}$$

This results in three sets of c'_{ij0}: one for longitudinal moduli, another for off-diagonal and shear, and a third for mixed elastic constants (Fig. 2.10). The experimental values of the pressure derivatives of cubic elements fall near the expected trends, which account for the greater pressure derivatives of the longitudinal moduli and intermediate values for off-diagonal and shear. Of the patterns apparent in these results, only the systematically larger values of the off-diagonal pressure derivatives as compared with the shear are not explained. Similar results have been found in oxides and silicates [60].

2.4.3.2. *Elastic Instabilities*

Silica provides an excellent example of a pressure-induced elastic instability that can precisely be linked to a phase transformation [52, 61, 62]. The transformation is from the stishovite phase to a phase with a $CaCl_2$-type structure which occurs near 47 GPa. In stishovite, C_{11} increases slowly with pressure up to 40 GPa and then decreases on further compression whereas C_{12} grows at an increasing rate thereby causing $C_{11} - C_{12}$

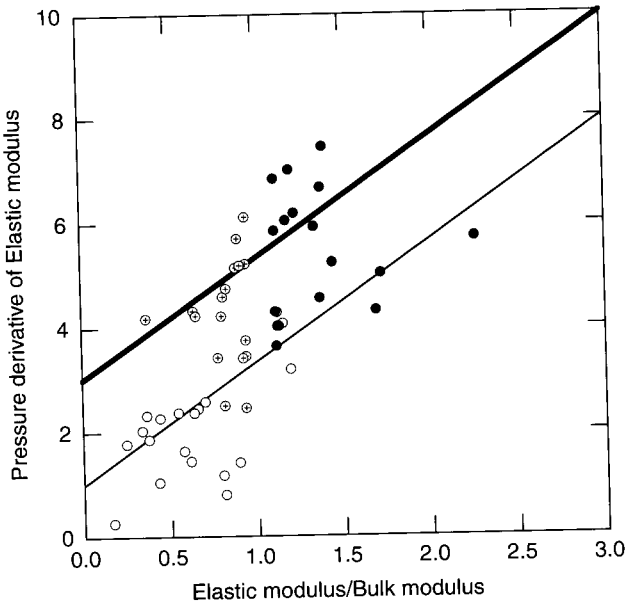

Fig. 2.10. Elastic properties of several cubic elements (Li, Na, K, Rb, Fe, Ni, Cu, Nb, Pd, Ag, Ta, Au, Al, C, Si, Ge, Pb) for (filled) longitudinal, (crosses) off-diagonal, and (open) shear elastic constants compared with the predictions of the second-order truncation of the Eulerian finite strain theory: (bold) longitudinal constants, (light) shear and off-diagonal constants.

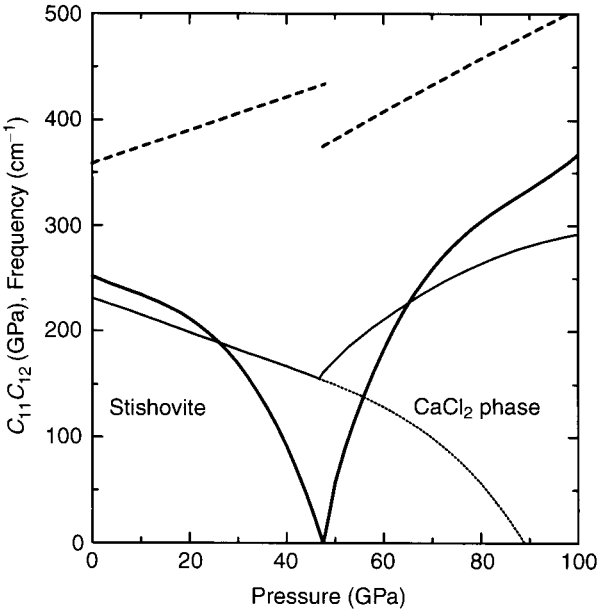

Fig. 2.11. Shear elastic modulus and Raman frequency of silica in the vicinity of the stishovite to $CaCl_2$ structure phase transition at 47 GPa according to LDA pseudo-potential calculations [60]: (bold solid) elastic constant $C_{11} - C_{12}$; (bold dashed) partial elastic constant $C_{11} - C_{12}$ (neglecting sublattice displacements); (light solid) frequency of the Raman B_{1g} mode; (light dashed) continuation of the Raman mode frequency in the (metastable) stishovite phase. From [60].

to vanish at ~47 GPa, the pressure for stishovite-to-$CaCl_2$ phase transition (Fig. 2.11). The $C_{11} - C_{12} = 0$ instability arises from a strong coupling between a shear strain of orthorhombic symmetry in the $a - b$ plane and the soft B_{1g} mode, discussed previously. The strain provides a deformation path that relates the lattices of the two structures (tetragonal stishovite and orthorhombic $CaCl_2$ phase) whereas the B_{1g} mode involves a rotation of SiO_6 octahedra around the c-axis that relates the two structures. The calculated modulus $C_{11} - C_{12}$ does not soften unless the sublattice displacements are accounted for (Fig. 2.11). While the frequency of the B_{1g} mode is softened considerably by 47 GPa, it does not vanish until much higher pressures (86 GPa), well beyond the stability field of stishovite.

2.4.3.3. Qualitative Changes in Anisotropy

The pressure derivatives of the elastic constants may vary widely even for a single phase. One consequence of this is that the elastic anisotropy may depend strongly on pressure. The pressure-induced change in anisotropy may be qualitative as well as quantitative; that is, the directions of fastest and slowest elastic wave propagation may reverse upon compression. An example is MgO (Fig. 2.12). Its anisotropy at first decreases with increasing pressure, vanishing near 15 GPa, and then increases upon further compression [17]. This behavior is consistent with experimental observations [14, 63]. The change in sign of the anisotropy factor, A, and the exchange between the fast and slow directions at ~15 GPa are determined by the ratio of the shear moduli C_{44} and c_s (which is greater than one below 15 GPa and less than one above 15 GPa). The fast S-wave propagation direction is [100] at zero pressure (corresponding to C_{44}) but it is [110] above 15 GPa (corresponding to c_s). Similar behavior is seen in other materials including ringwoodite, a spinel-structure mineral with Mg_2SiO_4 composition [64].

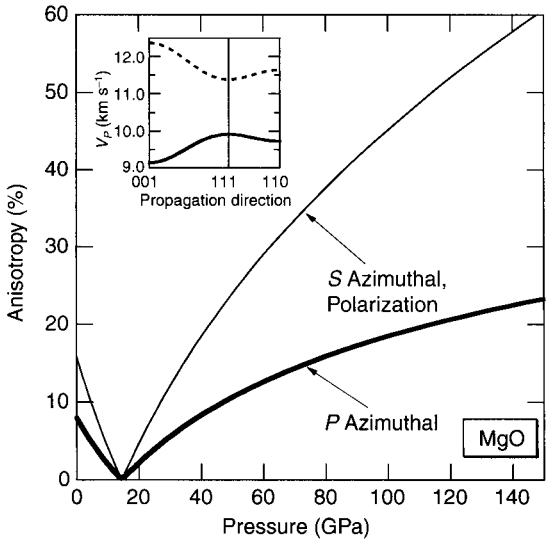

Fig. 2.12. Elastic anisotropy of MgO at high pressure according to LDA pseudo-potential calculations [17]. Azimuthal anisotropy is defined by $(V_{X\,\max} - V_{X\,\min})/V_X$ where X refers to $P-$ or S-waves, and V_X is the velocity averaged over all propagation directions. For cubic materials, polarization and S-wave azimuthal anisotropy are identical. The inset shows the P-wave velocity as a function of propagation direction at ambient pressure (lower curve) and at 30 GPa (upper curve). Modified from [17].

2.5. CONCLUSIONS

Density functional theory has opened up new frontiers in the study of the elastic constants of materials. It is now possible to compute partial and complete elastic constants of relatively complex materials (tens of atoms in the unit cell) efficiently. These calculations have illuminated important physics, especially at high pressure, including the importance of sublattice displacements, and the nature of elastic anisotropy. The first-principles investigation of elasticity at high temperature remains in its infancy although ab initio molecular dynamics and linear response methods are rapidly opening new frontiers. Other future directions in first-principles studies will no doubt include the elasticity of a-periodic materials, including glasses, liquids, and liquid crystals, and defective crystals. The interaction of defects with elastic and anelastic deformation will be important for gaining a better understanding of deformation at long time scales and over large strains.

References

This work supported by the National Science Foundation under grants EAR-9614790, EAR-9628199, and EAR-9973139.

1. Born, M., and Huang, K. (1954). *Dynamical Theory of Crystal Lattices*, Oxford: Oxford University Press.
2. Musgrave, M.J.P. (1970). *Crystal Acoustics*, San Francisco: Holden-Day.
3. Barron, T.H.K., and Klein, M.L. (1965). Second-order elastic constants of a solid under stress. *Proceedings of the Physical Society* **85**: 523–532.
4. Wallace, D.C. (1972). *Thermodynamics of Crystals*, 1st ed., New York: John Wiley & Sons.
5. Hohenberg, P., and Kohn, W. (1964). Inhomogeneous electron gas. *Physical Review* **136**: B864–B871.
6. Kohn, W., and Sham, L.J. (1965). Self-consistent equations including exchange and correlation effects. *Physical Review* **140**: A1133–A1138.
7. Cohen, M.L. (1984). Application of the pseudopotential model to solids. *Annual Reviews of Materials Science* **14**: 119–144.

8. Nielsen, O.H., and Martin, R. (1985). Quantum mechanical theory of stress and force. *Physical Review B* **32**: 3780–3791.
9. Car, R., and Parrinello, M. (1985). Unified approach for molecular dynamics and density-functional theory. *Physical Review Letters* **55**: 2471–2474.
10. Wentzcovitch, R.M., Martins, J.L., and Price, G.D. (1993). *Ab initio* molecular dynamics with variable cell shape: application to $MgSiO_3$ perovskite. *Physical Review Letters* **70**: 3947–3950.
11. Davies, G.F. (1974). Effective elastic moduli under hydrostatic stress—I. Quasi-harmonic theory. *Journal of Physics and Chemistry of Solids* **35**: 1513–1520.
12. Knittle, E., and Jeanloz, R. (1985). High-pressure x-ray-diffraction and optical-absorption studies of CsI. *Journal of the Physics and Chemistry of Solids* **46**: 1179–1184.
13. Marsden, J.E., and Hughes, T.J.R. (1983). *Mathematical Foundations of Elasticity*, Upper Saddle River, NJ: Prentice-Hall.
14. Duffy, T.S., Hemley, R.J., and Mao, H.K. (1995). Equation of state and shear-strength at multimegabar pressures—magnesium oxide to 227 GPa. *Physical Review Letters* **74**: 1371–1374.
15. Nye, J.F. (1985). *Physical Properties of Crystals: Their Representation by Tensors and Matrices*, 2nd ed., Oxford, UK: Oxford.
16. Birch, F. (1961). The velocity of compressional waves in rocks to 10 kilobars, Part 2. *Journal of Geophysical Research* **66**: 2199–2224.
17. Karki, B.B., *et al.* (1997). Structure and elasticity of MgO at high pressure. *American Mineralogist* **82**: 51–60.
18. Hill, R. (1952). The elastic behavior of a crystalline aggregate. *Proceedings of the Physical Society, London* **65A**: 349–354.
19. Watt, J.P., Davies, G.F., and O'Connell, R.J., (1976). The elastic properties of composite materials. *Reviews of Geophysics and Space Physics* **14**: 541–563.
20. Hashin, Z., and Shtrikman, S. (1962). A variational approach to the theory of the elastic behavior of polycrystals. *Journal of the Mechanics and Physics of Solids* **10**: 343–352.
21. Watt, J.P. (1987). Polyxstal: A fortran program to calculate average elastic properties of minerals from single-crystal data. *Computers and Geosciences* **13**: 441–462.
22. Karato, S. (1989). In *Rheology of solids and of the earth*, edited by Karato, S., and Toriumi, M. Oxford: Oxford University Press, pp. 393–422.
23. Wenk, H.-R. (1985). *Preferred Orientation in Deformed Metals and Rocks: An Introduction to Modern Texture Analysis*, Orlando: Academic Press.
24. Martin, J.W. (1975). Many-body forces in solids and Brugger elastic-constants 2. Inner elastic-constants. *Journal of Physics C—Solid State* **8**: 2858–2868.
25. Masters, T.G., and Shearer, P.M. (1995). In *Handbook of Physical Constants: Global Earth Physics*, edited by Ahrens, T.J. Washington, DC: American Geophysical Union, pp. 88–103.
26. Rivers, M.L., and Carmichael, I.S.E. (1987). Ultrasonic studies of silicate melts. *Journal of Geophysical Research* **92**: 9247–9270.
27. Hansen, J.-P., and McDonald, I.R. (1986). *Theory of Simple Liquids*, 2nd ed., London: Academic Press.
28. Nehring, J., and Saupe, A. (1971). Elastic theory of uniaxial liquid crystals. *Journal of Chemical Physics* **54**: 337.
29. Jeanloz, R., and Morris, S. (1986). Temperature distribution in the crust and mantle. *Annual Reviews of Earth and Planetary Science* **14**: 377–415.
30. Lundqvist, S., and March, N.H. (1987). *Theory of the Inhomogeneous Electron Gas*, London: Plenum Press.
31. Perdew, J.P., Burke, K., and Ernzerhof, M. (1996). Generalized gradient approximation made simple. *Physical Review Letters* **77**: 3865–3868.
32. Bagno, P., Jepsen, O., and Gunnarson, O. (1989). Ground-state properties of third-row elements with nonlocal density functionals. *Physical Review B* **40**: 1997–2000.
33. Hamann, D.R. (1996). Generalized gradient theory for silica phase transitions. *Physical Review Letters* **76**: 660–663.
34. Anderson, O.K. (1975). Linear methods in band theory. *Physical Review B* **12**: 3060–3083.
35. Wei, S.-H., and Krakauer, H. (1985). Local-density-functional calculations of the pressure-induced metallization of BaSe and BaTe. *Physical Review Letters* **55**: 1200–1203.
36. Stixrude, L., and Cohen, R.E. (1993). Stability of orthorhombic $MgSiO_3$-perovskite in the Earth's lower mantle. *Nature* **364**: 613–161.
37. Pickett, W.E. (1989). Pseudopotentials in condensed matter systems. *Comp. Phys. Rep.* **9**: 114–197.
38. Steinle-Neumann, G., Stixrude, L., and Cohen, R.E. (1999). First-principles elastic constants for the hcp transition metals Fe, Co, and Re at high pressure. *Physical Review B* **60**: 791–799.
39. Karki, B.B., Wentzcovitch, R.M., de Gironcoli, S., and Baroni, S. (1999). First principles determination of elastic anisotropy and wave velocities of MgO at lower mantle conditions. *Science* **286**: 1705–1707.
40. Ita, J.J., and Cohen, R.E. (1997). Effect of pressure on diffusion and vacancy formation in MgO from non-empirical free energy integrations. *Physical Review Letters* **79**: 3198–3201.

41. Gordon, R.G., and Kim, Y.S. (1972). Theory for the forces between closed-shell atoms and molecules. *Journal of Chemical Physics* **56**: 3122–3133.
42. Cohen, R.E., Boyer, L.L., and Mehl, M.J. (1987). Lattice dynamics of the potential induced breathing model: First principles phonon dispersion in the alkaline earth oxides. *Physical Review B* **35**: 5749–5760.
43. Wolf, G.H., and Bukowinski, M.S.T. (1988). Variational stabilization of the ionic charge densities in the electron-gas theory of crystals: Applications to MgO and CaO. *Physics and Chemistry of Minerals* **15**: 209–220.
44. Slater, J.C. (1951). A simplification of the Hartree-Fock method. *Physical Review* **81**: 385–390.
45. Cohen, R.E., Mehl, M.J., and Papacontantopoulos, D.A. (1994). Tight-binding total energy method for transition and noble metals. *Physical Review B* **50**: 14694–14697.
46. Cohen, R.E., Stixrude, L., and Wasserman, E. (1997). Tight-binding computations of elastic anisotropy of Fe, Xe, and Si under compression. *Physical Review B* **56**: 8575–8589.
47. Birch, F. (1952). Elasticity and constitution of the earth's interior. *Journal of Geophysical Research* **57**: 227–286.
48. Stixrude, L. (2000). In *Mineral Physics and Seismic Tomography*, edited by Karato, S., Liebermann, R.C., Masters, T.G., and Stixrude, L. Washington, DC: American Geophysical Union, in press.
49. Hazen, R.M., and Finger, L.W. (1979). Bulk modulus-volume relationship for cation-anion polyhedra. *Journal of Geophysical Research* **84**: 6723–6728.
50. Bukowinski, M.S.T. (1980). Pressure effect on bonding in MgO. *Journal of Geophysical Research* **85**: 285–292.
51. Isaak, D.G., Cohen, R.E., and Mehl, M.E. (1990). Calculated elastic constants and thermal properties of MgO at high pressures and temperatures. *Journal of Geophysical Research* **95**: 7055–7067.
52. Karki, B.B., *et al.* (1997). *Ab initio* studies of high-pressure structural transformations in silica. *Physical Review B* **55**: 3465–3471.
53. Karki, B.B., *et al.* (1997). *Ab initio* elasticity of three high-pressure polymorphs of silica. *Geophysical Research Letters* **24**: 3269–3272.
54. Pettifor, D.G. (1987). A quantum-mechanical critique of the miedema rules for alloy formation. *Solid State Physics* **40**: 43–92.
55. Harrison, W.A. (1980). *Electronic Structure and the Properties of Solids*, San Francisco: W. H. Freeman and Company.
56. Nastar, M., and WIllaime, F. (1995). Tight-binding calculation of the elastic constants of fcc and hcp transition metals. *Physical Review B* **51**: 6896–6907.
57. Stixrude, L., and Cohen, R.E. (1995). High pressure elasticity of iron and anisotropy of earth's inner core. *Science* **267**: 1972–1975.
58. Stixrude, L., Cohen, R.E., and Singh, D.J. (1994). Iron at high pressure: linearized augmented plane wave calculations in the generalized gradient approximation. *Physical Review B* **50**: 6442–6445.
59. Jeanloz, R. (1988). Universal equation of state. *Physical Review B* **38**: 805–807.
60. Karki, B.B., Stixrude, L., and Wentzcovitch, R.M. (2000). Elastic properties of major materials of earth's mantle from first principles. *Reviews of Geophysics* submitted.
61. Cohen, R.E. (1992). In *High-Pressure Research: Applications to Earth and Planetary Sciences*, edited by Syono, Y. and Manghnani, M.H. Tokyo: TERRAPUB pp. 425–431.
62. Kingma, K.J., Cohen, R.E., Hemley, R.J., and Mao, H.K. (1995). Transformation of stishovite to denser phase at lower-mantle pressures. *Nature* **374**: 243–245.
63. Sinogeikin, S.V., and Bass, J.D. (1999). Single-crystal elasticity of MgO at high pressure. *Physical Review B* **59**: R14141–R14144.
64. Kiefer, B., Stixrude, L., and Wentzcovitch, R.M. (1997). Elastic constants and anisotropy of Mg_2SiO_4 spinel at high pressure. *Geophysical Research Letters* **24**: 2841–2844.
65. Da Silva, C., Stixrude, L., and Wentzcovitch, R.M. (1997). Elastic constants and anisotropy of forsterite at high pressure. *Geophysical Research Letters* **24**: 1963–1966.